nature structural & molecular biology

Bilateral inhibition of HAUSP deubiquitinase by a viral interferon regulatory factor protein

Hye-Ra Lee[1,8], Won-Chan Choi[2,8], Stacy Lee[1], Jungwon Hwang[2,3], Eunha Hwang[4], Koushik Guchhait[2,5], Juergen Haas[6], Zsolt Toth[1], Young Ho Jeon[4,7], Tae-Kwang Oh[2], Myung Hee Kim[2,5] & Jae U Jung[1]

Herpesvirus-associated ubiquitin-specific protease (HAUSP) regulates the stability of p53 and the p53-binding protein MDM2, implicating HAUSP as a therapeutic target for tuning p53-mediated antitumor activity. Here we report the structural analysis of HAUSP with Kaposi's sarcoma–associated herpesvirus viral interferon (IFN) regulatory factor 4 (vIRF4) and the discovery of two vIRF4-derived peptides, vif1 and vif2, as potent and selective HAUSP antagonists. This analysis reveals a bilateral belt-type interaction that results in inhibition of HAUSP. The vif1 peptide binds the HAUSP TRAF domain, competitively blocking substrate binding, whereas the vif2 peptide binds both the HAUSP TRAF and catalytic domains, robustly suppressing its deubiquitination activity. Peptide treatments comprehensively blocked HAUSP, leading to p53-dependent cell-cycle arrest and apoptosis in culture and to tumor regression in xenograft mouse model. Thus, the virus has developed a unique strategy to target the HAUSP–MDM2–p53 pathway, and these virus-derived short peptides represent biologically active HAUSP antagonists.

The p53 pathway is partially abrogated in more than one-half of tumors through the inactivation of various signaling or effector components. Several recent studies have shown that the restoration of p53 activity alone can robustly induce tumor regression[1,2], asserting the p53 pathway as a prime target for new cancer-drug development. Accordingly, a number of strategies for targeting wild-type p53 have been designed. These include restoring p53 function by antagonizing its negative regulator, the E3 ubiquitin ligase MDM2, using peptides and small molecules that have been shown to induce p53-dependent suppression of tumor cell growth *in vitro* and *in vivo*[3–5]. However, MDM2 inhibition alone may not be sufficient to potently activate p53 in the *in vivo* tumor microenvironment[6].

It is well established that the level of p53 protein in cells is variable and is subtly regulated by ubiquitination and deubiquitination systems. HAUSP is a well-characterized deubiquitinase enzyme that has the ability to remove ubiquitin moieties from ubiquitinated substrates. It was initially identified as a binding partner of the herpes simplex virus (HSV) protein ICP0 that cooperatively facilitates viral replication[7]. Since then, further studies have shown that HAUSP can bind to various other substrates and is involved in the stress-response pathway, epigenetic silencing, neurodegenerative disorders and progression of infections by DNA viruses[8]. Additionally, HAUSP functions as a pivotal component of the p53–MDM2–MDMX signaling pathway, thus participating in the delicate balance that maintains p53 protein levels crucial for normal cellular homeostasis and diverse stress responses[9–11]. Notably, reduction or ablation of HAUSP leads to DNA damage–induced MDMX degradation and MDM2 instability, both of which robustly stabilize p53 (ref. 12).

Structural analyses reveal that both p53 and MDM2 specifically recognize the N-terminal tumor necrosis factor receptor–associated factor (TRAF)–like domain of HAUSP, and HAUSP-binding elements were mapped to a peptide fragment in the C terminus of p53 and to a short peptide region preceding the acidic domain of MDM2 (refs. 13,14). The cocrystal structures of the HAUSP TRAF–like domain in complex with these p53 and MDM2 short peptides demonstrate that the MDM2 peptide recognizes the same surface groove of HAUSP as that recognized by p53. However, the MDM2 peptide mediates more extensive interactions, indicating that MDM2, rather than p53, is the primary substrate of HAUSP under normal physiological conditions[13,14]. An Epstein-Barr virus (EBV) viral protein, Epstein-Barr nuclear antigen 1 (EBNA1), also binds the same region of HAUSP as that bound by the MDM2 and p53 peptides, competitively blocking these cellular interactions[15,16]. Thus, HAUSP seems to have multiple roles in regulating the p53–MDM2 pathway as well as in EBV-induced tumor cell survival, and it is therefore a potential chemotherapeutic target for p53-mediated suppression of tumor cell growth. In this report, we set out to answer the question of how viruses regulate HAUSP activity to escape the host's p53-mediated

[1]Department of Molecular Microbiology and Immunology, Keck School of Medicine, University of Southern California, Los Angeles, California, USA. [2]Division of Biosystems Research, Korea Research Institute of Bioscience and Biotechnology, Daejeon, Korea. [3]Department of Chemistry, Korea Advanced Institute of Science and Technology, Daejeon, Korea. [4]Division of Magnetic Resonance, Korea Basic Science Institute, Ochang, Chungbuk, Korea. [5]Biosystems and Bioengineering Program, University of Science and Technology, Daejeon, Korea. [6]Max-von-Pettenkofer-Institut, Ludwig-Maximilians-Universität München, München, Germany. [7]College of Pharmacy, Korea University, Jochiwon, Chungnam, Korea. [8]These authors contributed equally to this work. Correspondence should be addressed to T.-K.O. (otk@kribb.re.kr), M.H.K. (mhk8n@kribb.re.kr) or J.U.J. (jaeujung@usc.edu).

Received 26 March; accepted 19 August; published online 6 November 2011; doi:10.1038/nsmb.2142

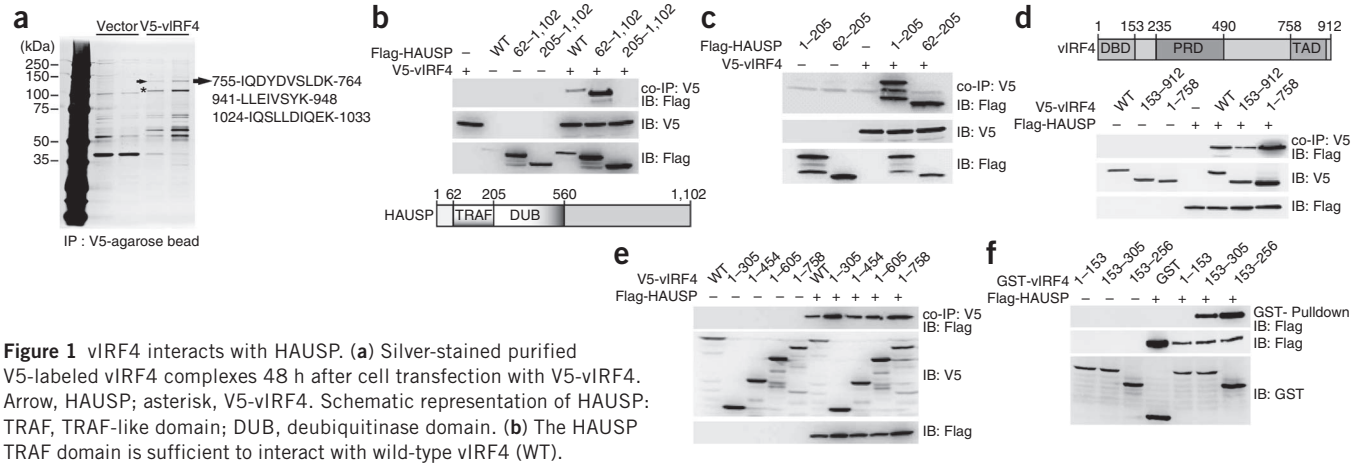

Figure 1 vIRF4 interacts with HAUSP. (**a**) Silver-stained purified V5-labeled vIRF4 complexes 48 h after cell transfection with V5-vIRF4. Arrow, HAUSP; asterisk, V5-vIRF4. Schematic representation of HAUSP: TRAF, TRAF-like domain; DUB, deubiquitinase domain. (**b**) The HAUSP TRAF domain is sufficient to interact with wild-type vIRF4 (WT). We transiently transfected 293T cells with the indicated constructs, carried out co-immunoprecipitation (co-IP) with an anti-V5 antibody, and immunoblotted (IB) with an anti-Flag antibody. (**c**) We subjected 293T cells transfected with the indicated constructs to co-IP and IB. (**d**) The central region of vIRF4 is required for HAUSP interaction. Schematic representation of vIRF4: DBD, DNA-binding domain; PRD, proline-rich domain; TAD, transactivation domain. We transfected 293T cells with the indicated constructs, followed by co-IP and IB. (**e**) Co-IP of HAUSP with wild-type vIRF4 or several vIRF4 mutants. We subjected 293T cells transfected with the indicated vIRF4 constructs along with HAUSP to IP and IB as in **b**. (**f**) $vIRF4_{153–256}$ is sufficient to bind to HAUSP. Cells were transfected with the indicated vIRF4 mutants in combination with empty vector or HAUSP, and subjected to glutathione S-transferase (GST) pulldown and IB with an anti-Flag antibody.

growth control. Here we describe the structural analysis of the Kaposi's sarcoma–associated herpesvirus (KSHV) vIRF4–HAUSP complex, and the discovery of two short viral peptides, vif1 and vif2, as potent, selective HAUSP antagonists.

RESULTS

Interaction between HAUSP and vIRF4 and complex structure

To study the HAUSP interaction network in KSHV (a γ-2 herpesvirus), we performed a yeast two-hybrid screen with a KSHV library[17] and MS analysis. Both studies independently discovered a previously unreported interaction between HAUSP and vIRF4 (**Fig. 1a**). Detailed binding assays indicated that the HAUSP TRAF domain ($HAUSP_{62–205}$) interacts specifically with $vIRF4_{153–256}$ (**Fig. 1b–f**). An isothermal titration calorimetry (ITC) assay revealed a robust interaction between $HAUSP_{62–205}$ and $vIRF4_{153–256}$, with a K_d of 76 nM; this K_d value is markedly higher than those reported for other HAUSP TRAF domain–binding substrates (K_d = 0.5–15 μM)[13–15,18] (**Supplementary Fig. 1a,b**).

To gain further insight into the molecular basis of the HAUSP–vIRF4 interaction, we crystallized the $HAUSP_{62–205}$–$vIRF4_{153–256}$ complex using an *in situ* proteolysis technique[19]. We determined the three-dimensional structure of this crystallized complex by the molecular replacement method using the HAUSP TRAF domain structure (PDB 2F1W[13]) as a search model, and refined to 1.6-Å resolution (**Fig. 2a** and **Table 1**). All residues of $HAUSP_{62–205}$ except Asp62 are included in the final model, whereas only 15 residues (Ser202–Met216) of vIRF4 are visible in the electron density map (**Supplementary Fig. 1c**). The overall structure of the HAUSP TRAF domain comprises a typical eight-stranded antiparallel β-sandwich fold (**Fig. 2a**) that forms a shallow groove in its surface structure (**Fig. 2b**, middle). We observed no significant conformational changes between the peptide-free (PDB 2F1W[13]) and vIRF4-bound TRAF domains, except that the C-terminal region of the TRAF domain was less extended upon vIRF4 binding (data not shown).

Detailed characterization of HAUSP TRAF–vIRF4 interaction

In contrast to previous studies that used synthetic or chimerically fused peptides of 4–10 amino acids in length in complex with the HAUSP TRAF domain[13–15,18], our *in situ* proteolysis treatment of the $HAUSP_{62–205}$–$vIRF4_{153–256}$ protein complex yielded a crystal structure with a markedly longer 15-residue vIRF4 peptide. The peptide consisted of an upstream (Ser202–Asn208) and a downstream (Ala211–Met216) region, which are linked by Glu209 and Gly210 (**Fig. 2a,b** and **Supplementary Fig. 1d**). The long peptide is positioned on the TRAF domain surface groove in a previously undescribed belt-type arrangement that threads through the left and right armholes (**Fig. 2b**, middle). This binding pattern is substantially different from that of other HAUSP substrates, which surround the left armhole of the TRAF domain (**Fig. 2b**, left).

The downstream region (Ala211–Met216) of vIRF4 corresponds to the peptides previously reported for p53, MDM2, MDMX and EBNA1 to complex with HAUSP TRAF (**Fig. 2b**, right). This region contains the well-conserved four-residue consensus sequence P/AXXS binding motif (**Fig. 2b**). The equivalent motif of vIRF4 consists of Ala211, Ser212, Thr213 and Ser214 and engages in extensive polar and nonpolar interactions (**Supplementary Fig. 1d**) with one side of the TRAF β-sheet, particularly the β7 strand (**Fig. 2a**). Overall, the interaction pattern between HAUSP TRAF and the downstream region of vIRF4 is similar to those previously reported for other peptides[13–15,18] (**Fig. 2b**). The upstream region (Ser202–Asn208) of vIRF4 binds to the HAUSP TRAF domain in a previously unreported extended conformation. This region participates in extensive interactions mainly with the other side of the β-sheet of the TRAF domain, especially the β6 strand (**Fig. 2a,b**). TRAF Arg153 seems to have a decisive and unique role in TRAF's interaction with the upstream region of the vIRF4 peptide (**Supplementary Fig. 1d**). On the other hand, vIRF4 Glu209 and Gly210 grasp the TRAF β6 and β7 strands (**Fig. 2a,b** and **Supplementary Fig. 1d**). These observations indicate that the distinctive upstream region of the vIRF4 peptide may be vital for stabilizing the interaction of the downstream consensus region with the HAUSP TRAF domain. Indeed, ITC analysis showed that deletion of this upstream region ($vIRF4_{209–216}$) results in a decrease in TRAF binding affinity by a factor of 25 compared with $vIRF4_{202–216}$ (**Supplementary Fig. 1a,b**), suggesting that vIRF4 uses a different interaction strategy from other HAUSP TRAF–binding cellular substrates as well as EBV EBNA1.

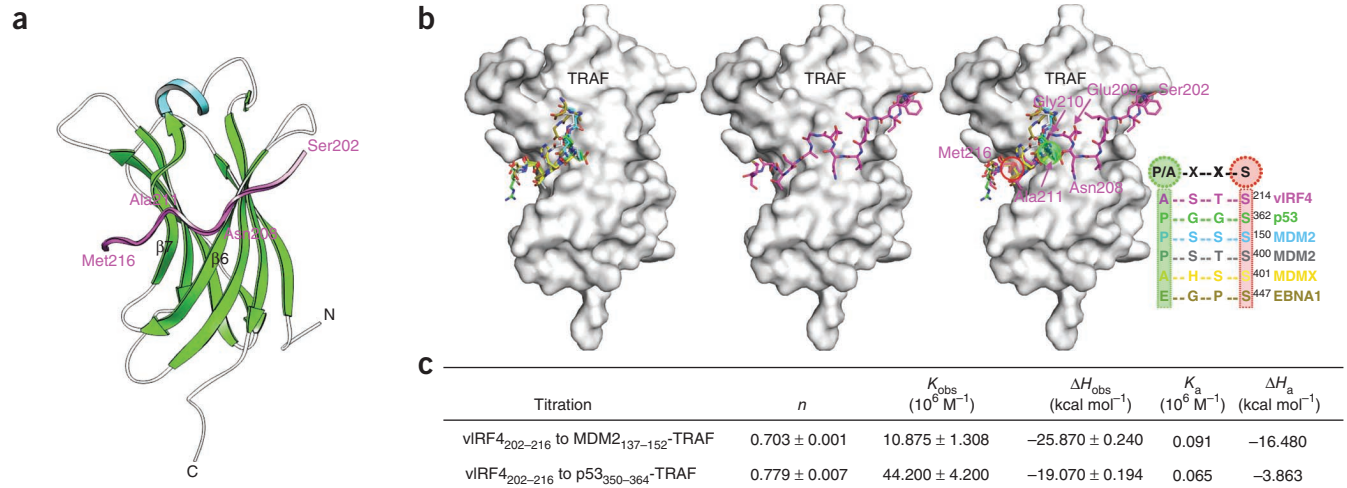

c

Titration	*n*	K_{obs} (10^6 M^{-1})	ΔH_{obs} (kcal mol^{-1})	K_a (10^6 M^{-1})	ΔH_a (kcal mol^{-1})
$vIRF4_{202–216}$ to $MDM2_{137–152}$-TRAF	0.703 ± 0.001	10.875 ± 1.308	–25.870 ± 0.240	0.091	–16.480
$vIRF4_{202–216}$ to $p53_{350–364}$-TRAF	0.779 ± 0.007	44.200 ± 4.200	–19.070 ± 0.194	0.065	–3.863
$vIRF4_{202–216}$ to $p53_{355–369}$-TRAF	0.761 ± 0.008	35.800 ± 3.400	–19.150 ± 0.203	0.067	–4.688

Figure 2 Structural basis for the interaction between HAUSP and vIRF4. (**a**) Ribbon representation of the vIRF4–HAUSP TRAF domain complex. The α-helix and β-sheets of the TRAF domain are shown in cyan and green, respectively. The β6 and β7 strands are indicated. The viral peptide (Ser202 to Met216) is magenta. (**b**) Distinctiveness of the HAUSP TRAF-vIRF4 interaction. Cellular substrates and EBV EBNA1 use a similar mode of interaction with HAUSP TRAF (left), whereas vIRF4 uses an unusual strategy for binding to TRAF (middle). Right, all target binding peptides are superimposed onto the HAUSP TRAF domain, including vIRF4 (magenta), p53 (green), MDM2 (cyan), MDM2 (gray), MDMX (yellow) and EBNA1 (olive). Residues in vIRF4 are labeled in magenta. The consensus sequence motif for each peptide is shown, and the most conserved residues are circled. (**c**) Thermodynamic parameters of competitive binding of vIRF4 with the TRAF domain against cellular substrates. Each cellular substrate peptide was first titrated into the TRAF domain, and the competitor $vIRF4_{202–216}$ was then titrated against each peptide.

HAUSP binding to $vIRF4_{202–216}$ versus other known substrates

ITC analysis with peptides containing the P/AXXS HAUSP-binding consensus sequence or the vIRF4 upstream region ($vIRF4_{202–216}$) showed that the $vIRF4_{202–216}$ peptide exhibited 28-fold to 40-fold tighter binding (K_d = 0.39 μM) to the TRAF domain than did peptides derived from MDM2 and p53 (**Supplementary Fig. 1a**,**b**). To evaluate whether vIRF4 competes with cellular substrates for binding to the HAUSP TRAF domain, we titrated each peptide ($MDM2_{137–152}$, $p53_{350–364}$ or $p53_{355–369}$) into the HAUSP TRAF domain, resulting in K_a values of 9.1×10^4 M^{-1}, 6.5×10^4 M^{-1} and 6.7×10^4 M^{-1}, respectively (**Fig. 2c**). When we subsequently titrated $vIRF4_{202–216}$ against HAUSP cellular substrates as a competitor, the observed association constant (K_{obs}) of each titration was markedly increased to 10.9×10^6 M^{-1}, 44.2×10^6 M^{-1} and 35.8×10^6 M^{-1}, respectively. These results indicate a considerably tighter interaction between the HAUSP TRAF domain and $vIRF4_{202–216}$ compared to HAUSP's interaction with its cellular substrates MDM2 and p53 (**Fig. 2c** and **Supplementary Fig. 2a**).

To further gauge the competitive nature of vIRF4 binding, we incubated the TRAF domain with an equimolar amount of $vIRF4_{153–216}$ in the presence of a five-fold molar excess of $MDM2_{137–152}$, followed by size-exclusion chromatography analysis. The $vIRF4_{153–216}$ peptide still formed a stable complex with TRAF even in the presence of a five-fold molar excess of MDM2 peptide (**Supplementary Fig. 2b**). This competitive nature of the $vIRF4_{153–216}$ peptide is probably due to its upstream region because the HAUSP binding affinity of the upstream region–deleted $vIRF4_{209–216}$ peptide (K_d = 9.57 μM) was comparable to that of $MDM2_{137–152}$ (K_d = 11.06 μM), $p53_{350–364}$ (K_d = 15.46 μM) and $p53_{355–369}$ (K_d = 15.46 μM) (**Supplementary Fig. 1b**).

NMR analysis of the HAUSP–vIRF4 interaction

The ITC analysis results revealed that, whereas the TRAF binding affinity (K_d = 0.54 μM) of $vIRF4_{153–216}$ was comparable to that of $vIRF4_{202–216}$, the C-terminally extended $vIRF4_{153–256}$ showed a seven-fold higher affinity (K_d = 0.076 μM). $vIRF4_{153–256/\Delta 202–216}$ (K_d = 3.45 μM) led to a substantial reduction in TRAF binding affinity, whereas $vIRF4_{153–256/\Delta 202–216/\Delta 237–256}$ (K_d = 4.03 μM) had no further effect (**Supplementary Fig. 1b**). Taken together, these results indicate that, in addition to $vIRF4_{202–216}$, the $vIRF4_{217–236}$ sequence has an important role in TRAF binding.

Table 1 X-ray data collection and refinement statistics

	$HAUSP_{62–205}$–$vIRF4_{153–256}$ complex
Data collection	
Space group	$P3_221$
Cell dimensions	
a, *b*, *c* (Å)	72.46, 72.46, 53.84
Resolution (Å)	1.60 (1.66–1.60)[a]
R_{sym}	0.061 (0.266)
$I / \sigma I$	65.2 (11.9)
Completeness (%)	100 (100)
Redundancy	21.7 (21.8)
Refinement	
Resolution (Å)	30.0–1.60
No. reflections	20,747
R_{work} / R_{free}	0.158 / 0.174
No. atoms	1,560
Protein (HAUSP–vIRF4)	1,216 / 106
Water	106
B-factors	14.81
Protein (HAUSP–vIRF4)	12.85 / 14.76
Water	24.85
R.m.s. deviations	
Bond lengths (Å)	0.008
Bond angles (°)	1.131

[a]Values in parentheses are for the highest-resolution shell.

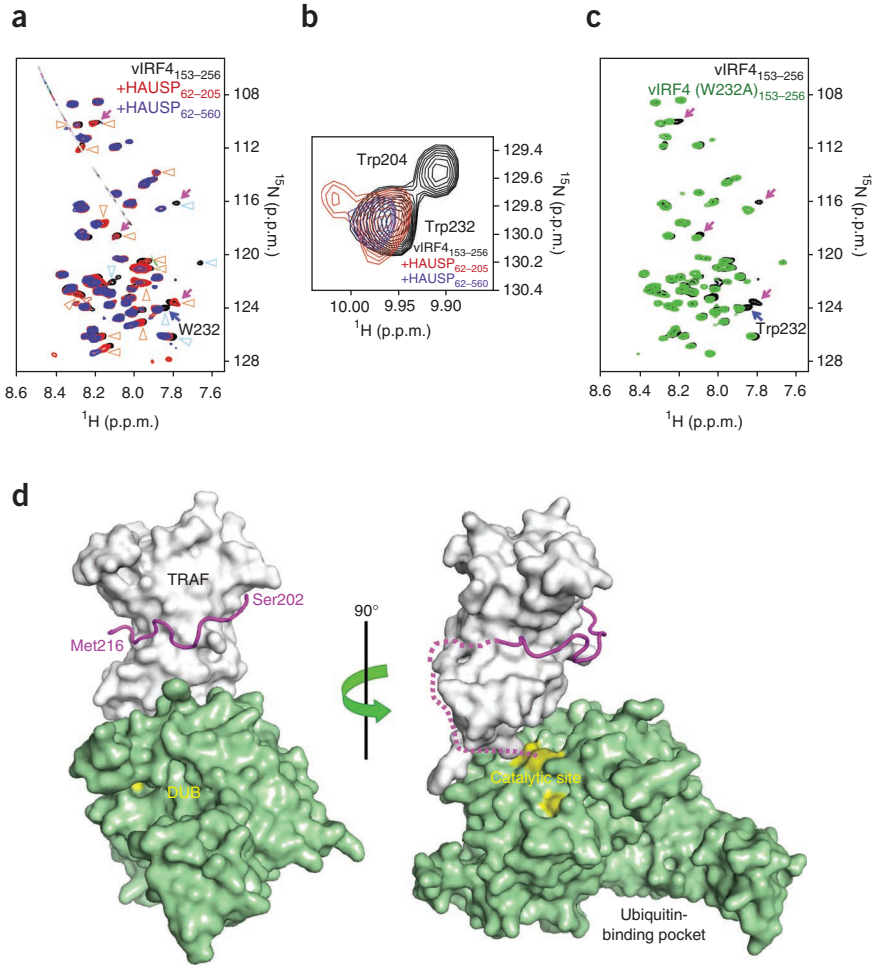

Figure 3 Bilateral interaction of vIRF4 with HAUSP. (**a**) NMR analysis of the interaction between the vIRF4 peptide and the HAUSP TRAF-DUB domain. Shown is the backbone amide region of the 2D ^{1}H-^{15}N correlation spectra of vIRF4$_{153–256}$ in the presence of an equimolar amount of HAUSP$_{62–205}$ (red) or HAUSP$_{62–560}$ (blue). The ^{1}H-^{15}N spectrum of free vIRF4$_{153–256}$ is shown in black. Blue triangles signal changes of vIRF4$_{153–256}$ observed upon binding of HAUSP$_{62–205}$. Orange triangles show additional changes detected upon binding of HAUSP$_{62–560}$. Magenta arrows indicate residues close to vIRF4 Trp232. (**b**) Signal changes of the tryptophan ε-NH protons upon interaction with HAUSP$_{62–205}$ (red) or HAUSP$_{62–560}$ (blue). Free vIRF4$_{153–256}$ is represented in black contours (see also **Supplementary Fig. 3a**). (**c**) The Trp232 backbone assignment. Superposition of the ^{1}H-^{15}N correlation spectra of free vIRF4$_{153–256}$ (black) and vIRF4 (W232A)$_{153–256}$ (green). Residues located close to Trp232 were identified by comparing the two spectra (magenta arrows). The blue arrow indicates the assigned Trp232 backbone (see also **Supplementary Fig. 3b**). (**d**) Proposed molecular interaction scheme between HAUSP and two different vIRF4-derived peptides. This model is based on the vIRF4–TRAF complex structure from the present study and the HAUSP structure containing the TRAF and DUB domains (PDB 2F1Z[13]). The vIRF4$_{202–216}$ peptide is shown as a magenta loop, and the vIRF4$_{217–236}$ peptide is depicted as a magenta short-dashed line. The catalytic triad (yellow) is highlighted in the catalytic site. The ubiquitin binding pocket is indicated.

To further dissect these ITC results, we analyzed NMR chemical-shift perturbations of vIRF4$_{153–256}$ in the presence of HAUSP$_{62–205}$ (TRAF domain) or HAUSP$_{62–560}$ (TRAF and deubiquitinase (DUB) domain). **Figure 3a** shows the superposition of the 2D ^{1}H-^{15}N correlation spectra of vIRF4$_{153–256}$ in the absence and presence of each HAUSP fragment. We observed signal changes (blue) of vIRF4$_{153–256}$ upon binding of HAUSP$_{62–205}$ (red) compared to free vIRF4$_{153–256}$ (black), and we detected additional changes (orange) upon binding of

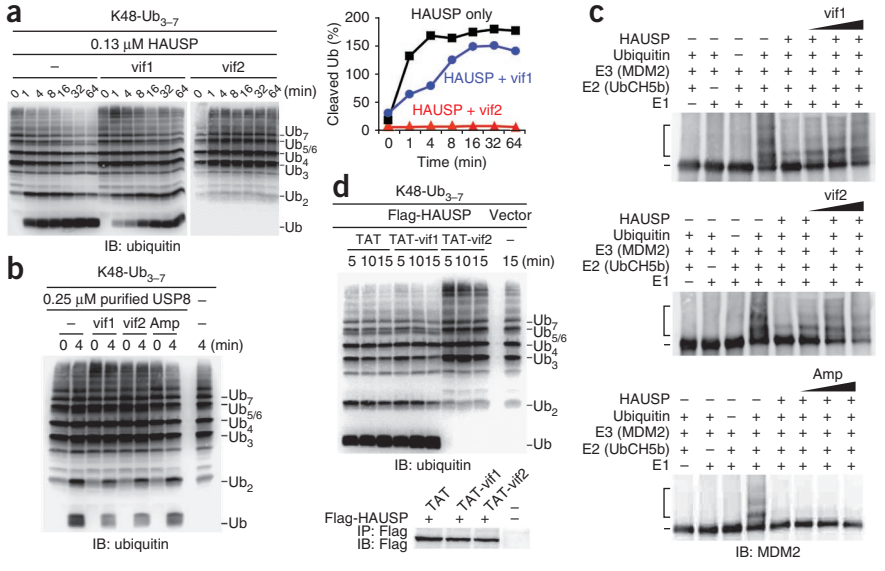

Figure 4 Effect of vIRF4 peptides on HAUSP DUB enzymatic activity. (**a**) Effect of vif1 and vif2 peptides on HAUSP DUB activity toward ubiquitin chains. A time course (right) is shown measuring the appearance of cleaved mono- and diubiquitin reaction products, as determined by semiquantification of immunoblots (IB, left). (**b**) The vif1 and vif2 peptides cannot inhibit USP8 deubiquitinase enzymatic activity *in vitro*. Purified USP8 was premixed with the vif1, vif2 or Amp (nonspecific) peptide for 5 min and then subjected to an *in vitro* DUB assay with the K48-Ub$_{3–7}$ chain. (**c**) Effect of vif1 and vif2 peptides on HAUSP DUB activity toward ubiquitinated MDM2. Human recombinant purified MDM2 was incubated with purified E1, E2 and ubiquitin before the DUB assay. HAUSP preincubated with increasing concentrations of each peptide or HAUSP alone was incubated with ubiquitinated MDM2. (**d**) *Ex vivo* effect of the TAT-vif1 and TAT-vif2 peptides on HAUSP DUB activity. At 24 h after transfection with vector or Flag-tagged HAUSP, 293T cells were treated with 100 μM of each peptide for an additional 12 h, followed by immunoprecipitation (IP) with anti-Flag agarose beads and elution with Flag peptide. Purified HAUSP complexes were incubated with K48-Ub$_{3–7}$ chains for the indicated intervals. 1% of the IP complex was used as the input.

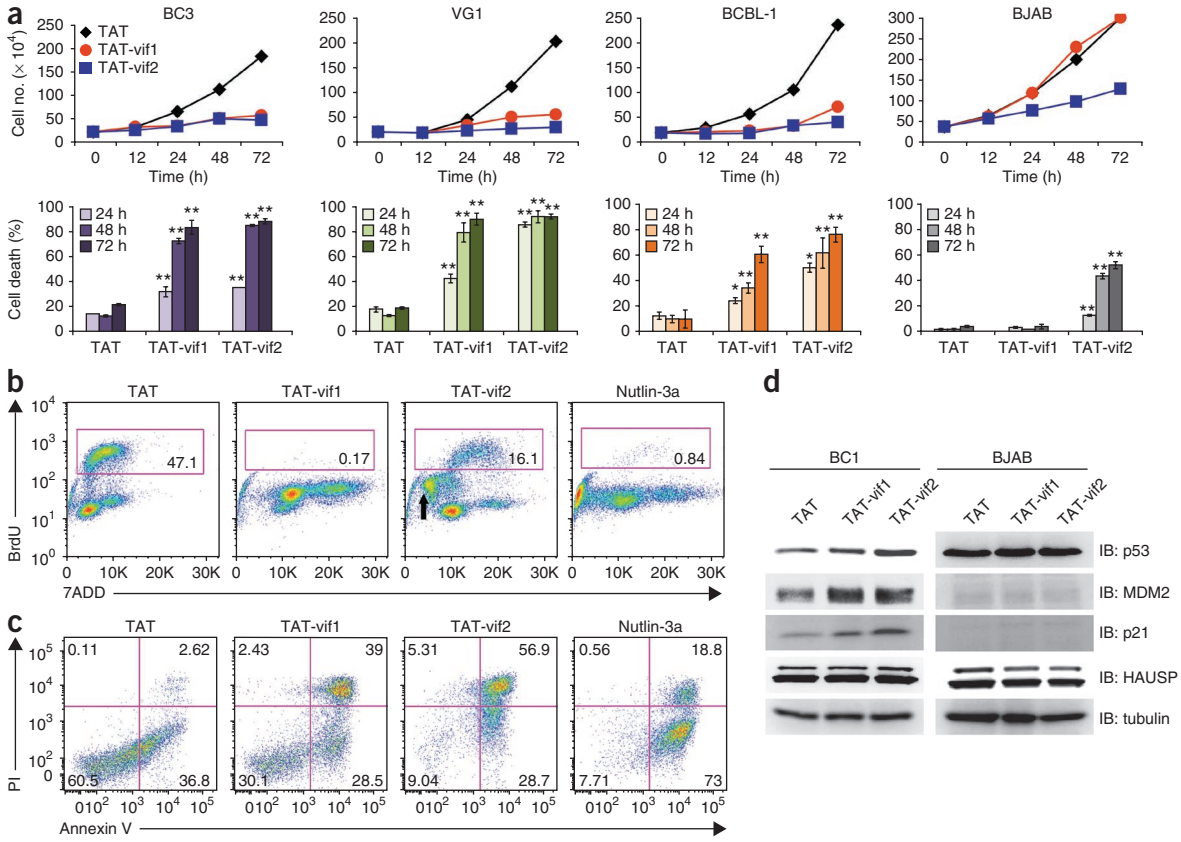

Figure 5 Cytotoxic effect of the TAT-vif1 or TAT-vif2 peptide on PEL cells. (**a**) Growth inhibition of PEL cells induced by the TAT-vif1 and TAT-vif2 peptides. BC3 (*TP53*$^{wt/wt}$), VG1 (*TP53*$^{wt/wt}$), BCBL-1 (*TP53*$^{wt/wt}$) and BJAB (*TP53*$^{mt/mt}$) cells were treated with a 100 μM concentration of each individual peptide for the indicated time periods. $*P < 0.01$, $**P < 0.001$. (**b**) TAT-vif1 and TAT-vif2 peptides induce cell-cycle arrest of PEL cells. BC1 (*TP53*$^{wt/wt}$) cells were treated with a 100-μm concentration of each peptide or 10 μM nutlin-3a for 48 h before pulse labeling with BrdU and 7-aminoactinomycin D (7-AAD) for and DNA content analysis. BrdU incorporation during the S phase is quantified as the percentage of stained cells. The sub-G_1 population in TAT-vif2 peptide–treated BC1 cells is denoted by an arrow. (**c**) TAT-vif1– and TAT-vif2–induced cell death of PELs. Apoptosis in BC1 cells was assessed by flow cytometry at 48 h after treatment with 10 μM nutlin-3a or a 100 μM concentration of each peptide by annexin V and propidium iodide (PI) staining. Numbers indicate the percentage of cells in each quadrant. (**d**) Effect of the TAT-vif1 and TAT-vif2 peptides on protein levels of p53 and its transcription targets. BC1 and BJAB cells were treated with the same dose as that used in **a**–**c** for 6 h. Aliquots of cell lysates containing 10 mg of protein were analyzed by immunoblotting (IB) with the indicated antibody.

HAUSP$_{62–560}$ (blue). The 2D ^{1}H-^{15}N correlation spectra and mutational analysis revealed that the ε-NH proton of vIRF4 Trp204 changes markedly upon binding of TRAF-containing HAUSP$_{62–205}$ (**Fig. 3b**, red, and **Supplementary Fig. 3a**), consistent with crystal structure data showing that Trp204 is located in the TRAF-binding region of vIRF4$_{202–216}$. In contrast, the ε-NH signal of Trp232 was perturbed by binding of the TRAF DUB–containing HAUSP$_{62–560}$ but not by binding of the TRAF-containing HAUSP$_{62–205}$ (**Fig. 3b**, blue). This latter result suggests that Trp232 is involved in the interaction of vIRF4 with the HAUSP DUB domain.

We performed selective isotope (^{15}N) labeling of Trp232 to further identify backbone amide signals derived from residues located near Trp232, by comparing vIRF4 and a W232A mutant (**Fig. 3c**, pink arrows, and **Supplementary Fig. 3b**). Results indicate that the residues near Trp232 are involved in binding to the HAUSP catalytic DUB domain (**Fig. 3a**). However, although vIRF4 and its peptide fragments (vIRF4$_{202–216}$ and vIRF4$_{220–236}$) were individually capable of interacting with HAUSP, neither peptide was able to bind to the HAUSP DUB domain alone (**Fig. 1b**, **Supplementary Fig. 4a** and data not shown), suggesting that a tight interaction with the N-terminal TRAF domain of HAUSP may be required for the binding of vIRF4 to the central DUB domain of HAUSP. These data suggest a bilateral mode of interaction between vIRF4 and HAUSP (**Fig. 3d**) wherein vIRF4$_{202–216}$ interacts with the HAUSP TRAF domain (primarily β6 and β7) with an unusually high binding affinity, and vIRF4$_{217–236}$ contacts the HAUSP DUB domain.

vIRF4 independently targets HAUSP and MDM2

As previously shown[20], vIRF4 expression considerably increases MDM2 levels and consequently decreases p53 levels in TREx/BCBL-1 vIRF4 cells expressing AU epitope–tagged vIRF4 (AU-vIRF4) in a tetracycline-inducible manner. Unlike vIRF4, the vIRF4$_{1–605}$ mutant, which cannot interact with MDM2, did not induce MDM2 stabilization and p53 degradation, whereas the vIRF4$_{Δ202–256}$ mutant, which cannot interact with HAUSP, increased MDM2 levels and marginally decreased p53 levels (**Supplementary Fig. 4b**,**c**). Consistent with these endogenous p53 amounts, vIRF4 markedly induced p53 ubiquitination, the vIRF4$_{Δ202–256}$ mutant did so to a lesser extent, and the vIRF4$_{1–605}$ mutant did not do so (**Supplementary Fig. 4c**). Thus, although vIRF4 interacts with both HAUSP and MDM2 to control p53 levels, the vIRF4–MDM2 interaction is more important in p53 downregulation than is the vIRF4–HAUSP interaction.

Inhibition of HAUSP DUB activity by vif1 and vif2 peptides

An *in vitro* DUB assay of immunopurified Flag-HAUSP complexes with Lys48-linked polyubiquitin chains of 3–7 ubiquitin moieties showed that vIRF4 effectively suppressed HAUSP DUB activity in a binding-dependent manner (**Supplementary Fig. 5a**). To further assess the effects of these vIRF4 short sequences on HAUSP enzymatic activity, we mixed the vIRF4 peptides corresponding to residues 202–216 (hereafter referred to as 'vif1') and 220–236 (hereafter referred to as 'vif2') with purified HAUSP and then subjected them to an *in vitro* DUB assay with Lys48- or Lys63-linked 3–7 polyubiquitin chains. We included an 'Amp' peptide derived from the amphipathic helix sequence of the herpesvirus saimiri Tip protein[21] as a negative control. The vif2 peptide markedly suppressed HAUSP DUB activity, whereas the vif1 peptide minimally inhibited activity, and the Amp peptide had no effect on HAUSP DUB activity (**Supplementary Fig. 5b**). Comparative kinetic analysis showed that whereas the vif1 peptide weakly attenuated HAUSP DUB activity, the vif2 peptide completely suppressed HAUSP DUB activity (**Fig. 4a**, right). These results strongly support the idea that the vif2 peptide (residues 220–236) directly contacts the catalytic domain of HAUSP and thereby inhibit its DUB activity. To confirm the specificity of the vif1 and vif2 peptides toward HAUSP, we conducted an *in vitro* DUB assay using USP8, which is in the same family as HAUSP[22]. In contrast to what was observed for HAUSP DUSB, neither the vif1 peptide nor the vif2 peptide inhibited USP8 DUB activity (**Fig. 4b**).

We then investigated whether the vif1 and vif2 peptides could inhibit HAUSP DUB activity against ubiquitinated substrates through substrate binding competition. To this end, we first generated ubiquitinated MDM2 using purified E1 (UBE1), E2 (UbcH5b) and E3 (MDM2) proteins and then performed an *in vitro* DUB assay using purified HAUSP alone or HAUSP preincubated with increasing amounts of each peptide (**Fig. 4c** and **Supplementary Fig. 5c**). The vif2 peptide efficiently blocked HAUSP enzymatic activity against both Lys48-linked polyubiquitin chains and ubiquitinated MDM2 (**Fig. 4a**,**c**). In contrast to its ineffectiveness against Lys48-linked polyubiquitin chains, the vif1 peptide effectively blocked HAUSP DUB activity when we used ubiquitinated MDM2 as a substrate (**Fig. 4c**). Incubation with the Amp peptide showed no effect on HAUSP DUB activity under the same conditions (**Fig. 4c**).

To further delineate the vIRF4 peptides' action *in vivo*, we fused the vif1 and vif2 peptides with the HIV-1 TAT protein transduction domain for intracellular delivery[23,24] and tested for their potential effects on *in vivo* HAUSP DUB activity. Consistent with the previous *in vitro* DUB assay, the TAT-vif2 peptide showed the strongest inhibitory activity toward *ex vivo* HAUSP enzymatic activity, but the TAT-vif1 peptide showed no effect under the same conditions (**Fig. 4d**). These results thus further corroborate the notion that vif1 interferes with HAUSP substrate binding, whereas vif2 inhibits HAUSP DUB activity.

Antitumor activity of TAT-vif1 and TAT-vif2 peptides

Because HAUSP has a pivotal role in the regulation of the p53 pathway[10,11], we investigated the potential effect of each peptide on KSHV-induced primary effusion lymphoma (PEL) tumor cell lines harboring wild-type p53 ($Tp53^{wt/wt}$)[25,26]. We included cell lines with mutated, nonfunctional p53 as controls. These results showed that time-dependent antiproliferative and cytotoxic activities differed depending on p53 status (**Fig. 5a**). In contrast to treatment with the HIV-1 TAT peptide, which showed no effect on cell proliferation and cell death, incubation of PELs with various concentrations (25 μM, 50 μM or 100 μM) of the TAT-vif2 peptide not only robustly suppressed cell proliferation, but also induced profound cell death. The TAT-vif1 peptide did the same but with a much weaker activity than did the TAT-vif2 peptide (**Supplementary Fig. 6a**). Notably, BJAB Burkitt lymphoma tumor cells carrying mutant p53 (ref. 27) continued to proliferate in the presence of the TAT-vif1 peptide and showed only minor growth retardation and cell death in the presence of the TAT-vif2 peptide (**Fig. 5a**). The prostate cancer cell lines LnCap ($Tp53^{wt/wt}$), PC3 ($Tp53^{-/-}$) and DU145 ($Tp53^{mt/mt}$)[28], which carry p53 genotypes with different degrees of function, showed the p53 dependence of TAT-vif1– and TAT-vif2–mediated cell death: LnCap cells, but not PC3 and DU145 cells, were highly susceptible to TAT-vif1– and TAT-vif2–mediated cell growth inhibition (**Supplementary Fig. 6b**). Taken together, these data show that both the vif1 and vif2 peptides have vigorous cell-killing activities against ($Tp53^{wt/wt}$)-containing tumor cells.

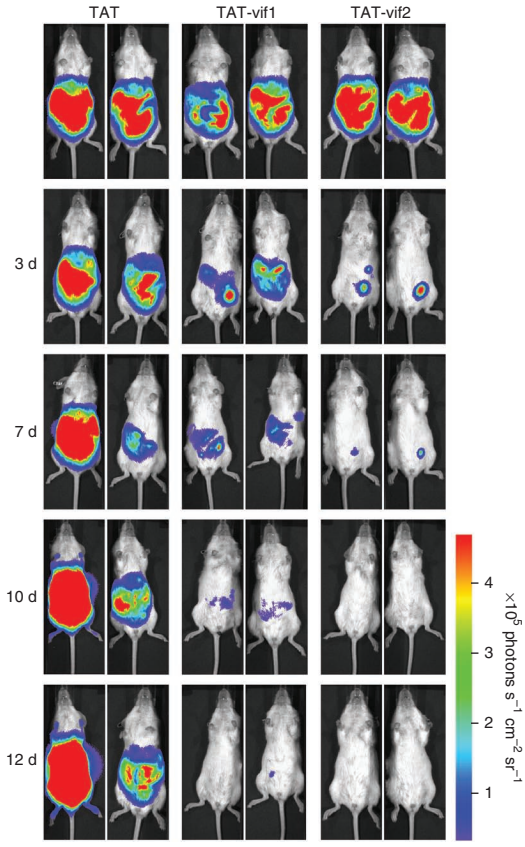

Figure 6 TAT-vif1 and TAT-vif2 induce tumor suppression *in vivo*. Time course of bioluminescent images of tumors formed from luciferase (Luc)-labeled BCBL-1 cells in NOD/SCID mice in response to intraperitoneal injection with 1 mg of TAT, TAT-vif1 or TAT-vif2 peptide for 2 weeks (see also **Supplementary Fig. 10**).

One of the main cellular consequences of p53 activation in proliferating cells is cell-cycle arrest through transcriptional upregulation of the cyclin-dependent kinase inhibitor p21, which causes G_1–S or G_2–M cell-cycle arrest[29,30]. Indeed, treatment of PEL cells with the TAT-vif1 or TAT-vif2 peptide markedly increased the G_1- and G_2–M-phase fraction and nearly completely depleted S-phase cells (**Fig. 5b** and **Supplementary Fig. 7**). Notably, we observed substantial sub-G_1 accumulation (reflecting cell death) in TAT-vif2–treated cells compared to TAT- or TAT-vif1–treated cells (**Fig. 5b** and **Supplementary Fig. 7**, arrows). Annexin V and propidium iodide staining assays showed that, although treatment with either the TAT-vif1 and TAT-vif2 peptides effectively induced apoptotic cell death in PEL cells carrying $Tp53^{wt/wt}$ compared to TAT treatment, the TAT-vif2 peptide more

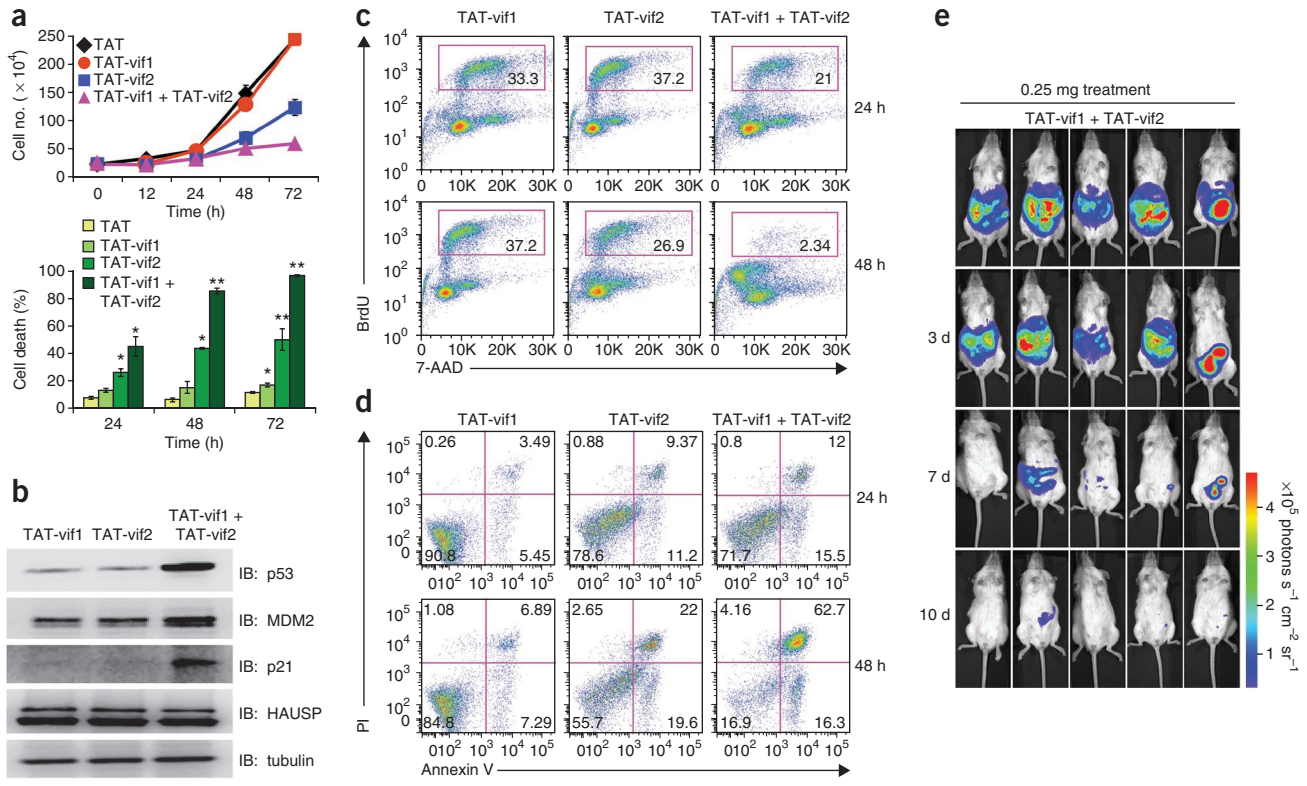

Figure 7 Combination therapeutic effects of a low dose of TAT-vif1 and TAT-vif2 peptides. (**a**) BCBL-1 cells were treated with a 25 μM concentration of each peptide, alone or in combination, for the indicated time periods. Cells were examined by trypan blue staining for cell death analysis or cell number counting for cell growth. $*P < 0.05$, $**P < 0.01$. (**b**) BCBL-1 cells were incubated for 6 h with a 25 μM concentration of TAT-vif1, TAT-vif2 or both. Whole-cell lysate (WCL) were subjected to SDS-PAGE followed by immunoblotting (IB) and were analyzed for p53, MDM2, p21 and HAUSP expression. (**c**) Asynchronously growing BCBL-1 cells were treated with a 25 μM concentration of the designated peptide or the combined peptides for the indicated time periods, before pulse labeling with BrdU and 7-aminoactinomycin D (7-AAD) for DNA content analysis. BrdU incorporation during the S phase is indicated as the percentage of stained cells. (**d**) Scatter plot of annexin V–FITC and propidium iodide (PI) flow cytometry of BCBL-1 cells after exposure to 25 μM peptide treatments for different time periods. Data are representative of three independent experiments. (**e**) After tumors were established in the NOD/SCID mice, 0.25 mg each of TAT-vif1 and TAT-vif2 peptide were injected together for 2 weeks. The tumors were measured by *in vivo* bioluminescence imaging.

rapidly and strongly induced apoptotic cell death than did the TAT-vif1 peptide (**Fig. 5c** and **Supplementary Fig. 8**). Treatment of nutlin-3a, which blocks the interaction between MDM2 and p53 and thus induces extensive apoptosis, also led to considerable cell death, comparable to either peptide treatment.

As the inhibition of HAUSP enzymatic activity stabilizes and activates p53, we examined the effect of each peptide on intracellular levels of p53 and its transcriptional targets p21, MDM2, NOXA and PUMA. Incubation of exponentially growing PEL, LnCap and DU145 tumor cells with either peptide for 6 h led to increased p53, p21, MDM2, PUMA and NOXA at different levels (**Fig. 5d** and **Supplementary Fig. 9**). By contrast, BJAB cells exposed to the same conditions showed no detectable changes in p53, MDM2 and p21 levels. Neither the vif1 nor vif2 peptide altered HAUSP levels in various PEL cells or in BJAB cells (**Fig. 5d** and **Supplementary Fig. 9**). These results show that the TAT-vif1 and TAT-vif2 peptides differentially affect the p53 pathway in cancer cells with functional ($Tp53^{wt/wt}$).

vif1 and vif2 peptides induce *in vivo* tumor regression

To evaluate the *in vivo* antitumor activity of the vif1 and vif2 peptides, we used NOD/SCID xenograft mice intraperitoneally injected with BCBL-1 luciferase cells as previously described[31–33]. After being injected with the tumor cells, all of the mice developed PEL, with evident distention and ascites in the peritoneal cavity as well as markedly increased luminescence (data not shown). We challenged mice with advanced PEL with 1 mg (equivalent to ~100 μM) of each peptide on days 3, 5, 7, and twice weekly for subsequent weeks by intraperitoneal injection. Treatment with the TAT-vif1 or TAT-vif2 peptide led to little or no traceable luminescence with marked tumor regression (**Fig. 6** and **Supplementary Fig. 10**). The TAT-vif2 peptide caused particularly efficient and powerful tumor regression. By contrast, tumors continuously advanced in mice that received TAT peptide injections (**Fig. 6** and **Supplementary Fig. 10**). The mice treated with the TAT-vif1 or TAT-vif2 peptide showed neither significant weight loss nor any gross abnormalities upon necropsy at the end of the treatment. These results collectively demonstrate the *in vivo* antitumor activity of the TAT-vif1 and TAT-vif2 peptides.

Combining vif1 and vif2 peptides increases antitumor activity

Owing to their bilateral inhibition of HAUSP activity, treatment with the TAT-vif1 and TAT-vif2 peptides combined caused considerable increases in antitumor activity: treatment with 25 μM TAT-vif1 and 25 μM TAT-vif2 was highly effective in inducing p53-dependent cell growth suppression, cell-cycle arrest and cell death, which was concordant with 100 μM treatment with the TAT-vif1 or TAT-vif2 peptides individually (**Fig. 7** and **Supplementary Fig. 11a**,**b**).

Furthermore, incubation of exponentially growing PELs cells with the TAT-vif1 and TAT-vif2 combination (25 μM of each) for 6 h robustly increased the levels of p53, p21 and MDM2 (**Fig. 7b** and **Supplementary Fig. 11c**). We observed marked tumor regression when we challenged NOD/SCID mice with advanced PEL with the TAT-vif1 and TAT-vif2 peptide combination (each at a dose of 0.25 mg, equivalent to ~25 μM) (**Fig. 7e**). These results demonstrate the enhanced antitumor activity of the TAT-vif1 and TAT-vif2 peptides when combined.

DISCUSSION

To bypass IFN- and p53-mediated irreversible cell-cycle arrest and apoptosis, and to complete its life cycle, KSHV has developed a unique mechanism for antagonizing cellular IFN- and p53-mediated host innate immune responses by incorporating viral homologs of cellular IFN regulatory factors (IRFs), called vIRFs. KSHV encodes four vIRFs in a cluster region that have two common biological functions contributing to host immune evasion: the inhibition of host IFN-mediated innate immunity and the deregulation of p53-mediated tumor-suppressive activity[34,35]. We previously reported that KSHV vIRF4 interacts with MDM2 through its C-terminal region, leading to inhibition of MDM2 autoubiquitination and stabilization of its protein levels, thus enhancing MDM2-mediated p53 degradation[20]. Here we show that vIRF4's actions with HAUSP and MDM2 are functionally and genetically separable, and that the vIRF4–MDM2 interaction is more important in downregulating p53 than is the vIRF4–HAUSP interaction. Thus, KSHV vIRF4 has evolved to target two components, MDM2 and HAUSP, of the p53 pathway to comprehensively suppress p53 function. This suggests that vIRF4 affects p53 tumor suppressor–mediated surveillance in a similar but distinct way from other viral proteins such as the EBV EBNA1. Last, it should be noted that vIRF4 circumvents host growth surveillance to enhance viral replication in infected cells in a manner reminiscent of HSV ICP0 and EBV EBNA1, which also direct HAUSP to promote viral replication and oncogenic processes, respectively[7,15]. Thus, HAUSP seems to be a common host target for human herpesviruses to support their life cycle and pathogenesis and hence is considered to be a potential target for antiviral therapy.

Using crystal structure analysis facilitated by *in situ* proteolysis, together with ITC assessment, we demonstrate that, although KSHV vIRF4 (residues ~210–216) binds to the same surface groove of the HAUSP TRAF domain as that recognized by MDM2 and p53, it uses a HAUSP interaction strategy different from that of MDM2 and p53. Beside residues 210–216, vIRF4 uses an additional short upstream region (residues 202–208) to interact extensively with the other side of the TRAF domain β-sheet, especially the β6 strand (**Fig. 2a**,**b**). It is this extra interaction property of vIRF4 that results in a much higher binding affinity to the HAUSP TRAF domain than those of MDM2 or p53.

Notably, in a study using a comparably designed peptide EBNA1$_{435–449}$ containing the P/AXXS motif and sequences equivalent to the vIRF4 upstream region, EBV EBNA1$_{435–449}$ showed a similar HAUSP TRAF binding affinity (K_d = 0.48 μM) to that of the vIRF4$_{202–216}$ peptide (K_d = 0.39 μM) (**Supplementary Fig. 1b**). However, NMR chemical shift mapping analysis showed that, unlike for the vIRF4 peptide, the EBNA1 sequences corresponding to the upstream region of the vIRF4 peptide did not affect its interaction with the HAUSP TRAF domain[15]. This result suggests that KSHV vIRF4 and EBV EBNA1 target HAUSP in similar but distinct manners. It is worth noting that EBNA1 is the only HAUSP TRAF–binding substrate with a charged side chain residue, Glu444, at the position of 'P/A' in the motif P/AXXS motif (**Supplementary Fig. 1b** and **Fig. 2b**). This residue seems to be crucial to how EBNA1 attains a higher binding affinity for HAUSP TRAF than do cellular substrates, as the Glu444 side chain interacts with the backbone amide and carbonyl group of Ser155 and Arg153 on the β6 strand, respectively, through bridging water molecules, as well as with the indole nitrogen of TRAF Trp165 (**Supplementary Fig. 1e**). Moreover, EBNA1 uses four backbone-backbone interactions with the Trp165–Asn169 residues on the TRAF β7 strand (**Supplementary Fig. 1e**), whereas cellular substrates use only two main chains to interact with the same TRAF strand (data not shown). As a consequence, the EBNA1 peptide may compete with cellular substrates even though they use similar HAUSP TRAF–binding patterns (**Fig. 2b**). These competences of EBNA1 may collectively result in an effect comparable to that seen with vIRF4$_{202–216}$ to manage HAUSP interactions with cellular substrates. Furthermore, independently of its inhibition of p53-mediated apoptosis, the EBNA1–HAUSP interaction is also involved in PML disruption to promote the survival of cells with DNA damage[36]. Thus, two human gamma herpesviruses have evolved to target and deregulate HAUSP function and its related pathways, but the consequences of their action may be substantially different.

Along with the structure of the HAUSP TRAF-DUB domain[13], our ITC, NMR and deubiquitinase enzyme analyses suggest that a peptide of ~17 amino acids (residues 216–232) may be long enough to stretch from the TRAF domain to the DUB domain of HAUSP, and additional sequences around residues 232–236 may directly contact the catalytic core site of HAUSP, resulting in the robust inhibition of its enzymatic activity. Because of these exceptional properties of vIRF4, the vif1 and vif2 peptides clearly posses two provocative and effective strategies that make them specific and robust HAUSP antagonists: the vif1 peptide binds to the HAUSP TRAF domain with the highest affinity among all reported substrates, blocking TRAF binding by cellular substrates, whereas the vif2 peptide seems to loosely bind the TRAF domain and the active catalytic site of the DUB domain of HAUSP, suppressing its DUB enzymatic activity. Consequently, the vif1 and vif2 peptides comprehensively suppress HAUSP activity, effectively restore p53-dependent apoptosis in wild-type p53-carrying cancer cells, and suppress tumor growth in mouse xenograft models. Our study not only provides strong evidence that the vif1 and vif2 peptides are ideal for abolishing HAUSP activity but also shows that they have the potential to be therapeutically beneficial reagents against p53 wild-type tumors. However, we should stress that the vIRF4 peptides studied here do not reflect the authentic biology of full-length vIRF4, which targets both HAUSP and MDM2 to comprehensively inactivate host p53-mediated surveillance. Thus, the therapeutic exploitation of the vIRF4 peptides as HAUSP inhibitors should be uncoupled from the biological function of vIRF4 as a survival factor against the host's immune surveillance programs.

Notably, because HAUSP contains a well-conserved catalytic core domain, it should therefore be a more tractable as a drug target than blocking the p53–MDM2–MDMX interaction. This is underscored by recent findings showing that HAUSP can be used to therapeutically target p53-independent apoptosis responses in certain tumors. For instance, the loss of HAUSP in colorectal cancer cells potentiates apoptotic cell death by inducing proteasomal degradation of DNMT1, further compounding the potential of HAUSP inhibition as an effective anticancer therapy[37–40]. Accordingly, because we cannot exclude the possibility that HAUSP regulates the function of other known or as-yet-unknown substrates involved in p53-independent apoptosis, our peptides may have additional off-target, p53-independent pro-apoptotic effects.

Our study shows that the vIRF4-derived short vif1 and vif2 peptides comprehensively suppress HAUSP activity, effectively restoring

p53-dependent apoptosis in wild-type p53-carrying cancer cells and suppressing tumor growth in a mouse xenograft model. Most notably, we herein report that the vif1 and vif2 peptides represent potential new chemotherapeutic molecules for anticancer therapies.

METHODS

Methods and any associated references are available in the online version of the paper at http://www.nature.com/nsmb/.

Accession codes. Protein Data Bank: Atomic coordinates and structure factors amplitudes of the HAUSP–vIRF4 complex have been deposited with accession code 2XXN.

Note: Supplementary information is available on the Nature Structural & Molecular Biology website.

ACKNOWLEDGMENTS

This work was partly supported by grants CA82057, CA31363, CA115284, CA147868, CA148616, DE019085, the Hastings Foundation, the Fletcher Jones Foundation, the William Lawrence and Blanche Hughes (WLBH) Foundation and the Global Research Laboratory (GRL) Program (K20815000001) from the National Research Foundation of Korea (J.U.J.); and the 21C Frontier Microbial Genomics and Applications Center Program and the National Research Foundation of Korea grant (NRF-M1AXA002-2010-0029767) funded by the Ministry of Education, Science and Technology, Korea (M.H.K.). We thank the staff at the 4A and 6B beamlines, Pohang Accelerator Laboratory, Korea, for help with data collection. We thank V. Lombardi, J. Jeong and J.S. Lee for their help. Finally, we thank all lab members for their support and discussions.

AUTHOR CONTRIBUTIONS

H.-R.L. performed all aspect of this study; W.-C.C., J.H. and M.H.K. did X-ray crystallographic and biochemical studies; S.L. and Z.T. assisted with the experimental design and collected the data; E.H. and Y.H.J. carried out NMR studies; K.G. did protein purification; J.H. provided the KSHV library; H.-R.L., W.-C.C., T.-K.O., M.H.K. and J.U.J. organized this study and wrote the manuscript. All authors discussed the results and commented on the manuscript.

COMPETING FINANCIAL INTERESTS

The authors declare no competing financial interests.

Published online at http://www.nature.com/nsmb/.
Reprints and permissions information is available online at http://www.nature.com/reprints/index.html.

1. Martins, C.P., Brown-Swigart, L. & Evan, G.I. Modeling the therapeutic efficacy of p53 restoration in tumors. *Cell* **127**, 1323–1334 (2006).
2. Ventura, A. *et al.* Restoration of p53 function leads to tumour regression *in vivo*. *Nature* **445**, 661–665 (2007).
3. Brown, C.J., Cheok, C.F., Verma, C.S. & Lane, D.P. Reactivation of p53: from peptides to small molecules. *Trends Pharmacol. Sci.* **32**, 53–62 (2011).
4. Lain, S. *et al.* Discovery, *in vivo* activity, and mechanism of action of a small-molecule p53 activator. *Cancer Cell* **13**, 454–463 (2008).
5. Yang, Y. *et al.* Small molecule inhibitors of HDM2 ubiquitin ligase activity stabilize and activate p53 in cells. *Cancer Cell* **7**, 547–559 (2005).
6. Wade, M., Wang, Y.V. & Wahl, G.M. The p53 orchestra: Mdm2 and Mdmx set the tone. *Trends Cell Biol.* **20**, 299–309 (2010).
7. Everett, R.D. *et al.* A novel ubiquitin-specific protease is dynamically associated with the PML nuclear domain and binds to a herpesvirus regulatory protein. *EMBO J.* **16**, 1519–1530 (1997).
8. Lee, J.T. & Gu, W. The multiple levels of regulation by p53 ubiquitination. *Cell Death Differ.* **17**, 86–92 (2010).
9. Brooks, C.L., Li, M., Hu, M., Shi, Y. & Gu, W. The p53–Mdm2–HAUSP complex is involved in p53 stabilization by HAUSP. *Oncogene* **26**, 7262–7266 (2007).
10. Cummins, J.M. & Vogelstein, B. HAUSP is required for p53 destabilization. *Cell Cycle* **3**, 689–692 (2004).
11. Cummins, J.M. et al. Tumour suppression: disruption of HAUSP gene stabilizes p53. *Nature* **428**, 428 (2004).
12. Meulmeester, E. *et al.* Loss of HAUSP-mediated deubiquitination contributes to DNA damage-induced destabilization of Hdmx and Hdm2. *Mol. Cell* **18**, 565–576 (2005).
13. Hu, M. *et al.* Structural basis of competitive recognition of p53 and MDM2 by HAUSP/USP7: implications for the regulation of the p53–MDM2 pathway. *PLoS Biol.* **4**, e27 (2006).
14. Sheng, Y. *et al.* Molecular recognition of p53 and MDM2 by USP7/HAUSP. *Nat. Struct. Mol. Biol.* **13**, 285–291 (2006).
15. Saridakis, V. *et al.* Structure of the p53 binding domain of HAUSP/USP7 bound to Epstein-Barr nuclear antigen 1 implications for EBV-mediated immortalization. *Mol. Cell* **18**, 25–36 (2005).
16. Holowaty, M.N. *et al.* Protein profiling with Epstein-Barr nuclear antigen-1 reveals an interaction with the herpesvirus-associated ubiquitin-specific protease HAUSP/USP7. *J. Biol. Chem.* **278**, 29987–29994 (2003).
17. Uetz, P. *et al.* Herpesviral protein networks and their interaction with the human proteome. *Science* **311**, 239–242 (2006).
18. Sarkari, F. *et al.* Further insight into substrate recognition by USP7: structural and biochemical analysis of the HdmX and Hdm2 interactions with USP7. *J. Mol. Biol.* **402**, 825–837 (2010).
19. Dong, A. *et al. In situ* proteolysis for protein crystallization and structure determination. *Nat. Methods* **4**, 1019–1021 (2007).
20. Lee, H.R. *et al.* Kaposi's sarcoma-associated herpesvirus viral interferon regulatory factor 4 targets MDM2 to deregulate the p53 tumor suppressor pathway. *J. Virol.* **83**, 6739–6747 (2009).
21. Min, C.K. *et al.* Role of amphipathic helix of a herpesviral protein in membrane deformation and T cell receptor downregulation. *PLoS Pathog.* **4**, e1000209 (2008).
22. Komander, D., Clague, M.J. & Urbe, S. Breaking the chains: structure and function of the deubiquitinases. *Nat. Rev. Mol. Cell Biol.* **10**, 550–563 (2009).
23. Wadia, J.S., Stan, R.V. & Dowdy, S.F. Transducible TAT-HA fusogenic peptide enhances escape of TAT-fusion proteins after lipid raft macropinocytosis. *Nat. Med.* **10**, 310–315 (2004).
24. Gump, J.M. & Dowdy, S.F. TAT transduction: the molecular mechanism and therapeutic prospects. *Trends Mol. Med.* **13**, 443–448 (2007).
25. Petre, C.E., Sin, S.H. & Dittmer, D.P. Functional p53 signaling in Kaposi's sarcoma-associated herpesvirus lymphomas: implications for therapy. *J. Virol.* **81**, 1912–1922 (2007).
26. Katano, H., Sato, Y. & Sata, T. Expression of p53 and human herpesvirus-8 (HHV-8)-encoded latency-associated nuclear antigen with inhibition of apoptosis in HHV-8-associated malignancies. *Cancer* **92**, 3076–3084 (2001).
27. Bhatia, K. *et al.* Hemi- or homozygosity: a requirement for some but not other p53 mutant proteins to accumulate and exert a pathogenetic effect. *FASEB J.* **7**, 951–956 (1993).
28. Zhang, R., Wang, H. & Agrawal, S. Novel antisense anti-MDM2 mixed-backbone oligonucleotides: proof of principle, *in vitro* and *in vivo* activities, and mechanisms. *Curr. Cancer Drug Targets* **5**, 43–49 (2005).
29. Kruse, J.P. & Gu, W. Modes of p53 regulation. *Cell* **137**, 609–622 (2009).
30. Bunz, F. *et al.* Requirement for p53 and p21 to sustain G2 arrest after DNA damage. *Science* **282**, 1497–1501 (1998).
31. Keller, S.A. *et al.* NF-kappaB is essential for the progression of KSHV- and EBV-infected lymphomas *in vivo*. *Blood* **107**, 3295–3302 (2006).
32. Lee, J.S. *et al.* FLIP-mediated autophagy regulation in cell death control. *Nat. Cell Biol.* **11**, 1355–1362 (2009).
33. Wu, W., Rochford, R., Toomey, L., Harrington, W. Jr. & Feuer, G. Inhibition of HHV-8/KSHV infected primary effusion lymphomas in NOD/SCID mice by azidothymidine and interferon-alpha. *Leuk. Res.* **29**, 545–555 (2005).
34. Lee, H.R., Lee, S., Chaudhary, P.M., Gill, P. & Jung, J.U. Immune evasion by Kaposi's sarcoma-associated herpesvirus. *Future Microbiol.* **5**, 1349–1365 (2010).
35. Lee, H.R., Kim, M.H., Lee, J.S., Liang, C. & Jung, J.U. Viral interferon regulatory factors. *J. Interferon Cytokine Res.* **29**, 621–627 (2009).
36. Sivachandran, N., Sarkari, F. & Frappier, L. Epstein-Barr nuclear antigen 1 contributes to nasopharyngeal carcinoma through disruption of PML nuclear bodies. *PLoS Pathog.* **4**, e1000170 (2008).
37. Du, Z. *et al.* DNMT1 stability is regulated by proteins coordinating deubiquitination and acetylation-driven ubiquitination. *Sci. Signal.* **3**, ra80 (2010).
38. De Marzo, A.M. *et al.* Abnormal regulation of DNA methyltransferase expression during colorectal carcinogenesis. *Cancer Res.* **59**, 3855–3860 (1999).
39. Agoston, A.T. *et al.* Increased protein stability causes DNA methyltransferase 1 dysregulation in breast cancer. *J. Biol. Chem.* **280**, 18302–18310 (2005).
40. Bronner, C. Control of DNMT1 abundance in epigenetic inheritance by acetylation, ubiquitylation, and the histone code. *Sci. Signal.* **4**, pe3 (2011).

ONLINE METHODS

Crystallization, data collection and structure determination. Crystallization trials were carried out using an *in situ* proteolysis technique[19]. The purified $HAUSP_{62–205}$–$vIRF4_{153–256}$ complex (50 mg ml^{-1}) was mixed with trypsin (1 mg ml^{-1}) in a 100:1 (v/v) ratio. The protease-treated protein complexes were used immediately for crystallization trials. Crystals were grown for 1 week under conditions of 5% (w/v) PEG 3350 and 0.2 M magnesium formate (pH 5.9) in an alternate reservoir containing a 1.5 M NaCl solution at 21 °C. Crystals were transferred to a cryoprotectant solution containing 30% (v/v) PEG 3350 and 0.2 M magnesium formate (pH 5.9), incubated for 2 h, and then retrieved and placed immediately in a −173 °C nitrogen gas stream. X-ray diffraction data were collected at 1.6-Å resolution on beamline 4A at the Pohang Accelerator Laboratory, Korea. All data were processed using the HKL2000 program suite[41]. The crystal of the protein complex belongs to space group $P3_221$. There is one complex in the asymmetric unit, with a packing density of ~2.26 $Å^3$ Da^{-1}, corresponding to an estimated solvent content of approximately 45.72%. The crystal structure was determined by molecular replacement using the MOLREP program[42]. The HAUSP TRAF domain structure (PDB 2F1W[13]) was used as a search model. The initial model was used as a guide to build the remainder of the protein manually into electron density maps with the program COOT[43]. Refinement was performed with REFMAC5 (ref. 44) and included the translation-libration-screw procedure. The final refined model resulted in R_{free} and R_{cryst} values of 0.174 and 0.158, respectively. The model contains 143 amino acids of the HAUSP TRAF domain, 15 residues of vIRF4 and 238 water molecules, and satisfies the quality criteria limits of the program PROCHECK[45]. The crystallographic data statistics are summarized in **Table 1**.

Additional methods. Information on cell culture, reagents plasmid constructions, the yeast-two hybrid screen, protein purification, immunoblotting and immunoprecipitation, ITC, NMR spectroscopy, the *in vitro* ubiquitination assay, the *in vitro* deubiquitination (DUB) assay, cell proliferation and viability assays, cell cycle and apoptosis assays, and *in vivo* bioimaging is available in the **Supplementary Methods**.

41. Otwinowski, Z. & Minor, W. Processing of X-ray diffraction data collected in oscillation mode. *Methods Enzymol.* **276**, 307–326 (1997).
42. Vagin, A. & Teplyakov, A. MOLREP: an automated program for molecular replacement. *J. Appl. Cryst.* **30**, 1022–1025 (1997).
43. Emsley, P. & Cowtan, K. Coot: model-building tools for molecular graphics. *Acta Crystallogr. D Biol. Crystallogr.* **60**, 2126–2132 (2004).
44. Murshudov, G.N., Vagin, A.A. & Dodson, E.J. Refinement of macromolecular structures by the maximum-likelihood method. *Acta Crystallogr. D Biol. Crystallogr.* **53**, 240–255 (1997).
45. Laskowski, R.A., Moss, D.S. & Thornton, J.M. Main-chain bond lengths and bond angles in protein structures. *J. Mol. Biol.* **231**, 1049–1067 (1993).